Tunable plasmon resonance coupling in coaxial gold nanotube arrays

Haiqing Xu (徐海清)[1,2*], Hongjian Li (李宏建)[2], and Gang Xiao (肖 刚)[1]

[1]*Department of Mathematics and Physics, Hunan Institute of Engineering, Xiangtan 411101, China*

[2]*College of Physics Science and Technology, Central South University, Changsha 410083, China*

[*]*Corresponding author: xu_hg2005@yahoo.com.cn*

Received October 15, 2012; accepted December 20, 2012; posted online March 8, 2013

The optical properties and plasmon resonance coupling of double coaxial gold nanotube arrays are investigated. The results show that the optical transmission is highly tunable by varying the thicknesses of the inner and outer nanotubes, the separation between the inner and outer nanotubes, and the dielectric parameters inside, between, and outside the two nanotubes. The shorter-wavelength transmission bands are very sensitive to the modification of the wall thickness of the outer nanotube, the separation, and the dielectric parameters between the double nanotubes. The dipole and multipolar plasmon modes are excited in our model. However, for small separation and refractive index, the dipole normal mode has a leading function in the transmission properties. Compared with the dipolar modes, the contribution of higher-order modes becomes larger as the parameters increase.

OCIS codes: 240.6680, 230.7370.

doi: 10.3788/COL201311.042401.

The transport of electromagnetic excitation along chains of noncontact metal nanoparticles has recently drawn attention[1−6]. The electromagnetic coupling between the particles in a chain delocalizes the surface plasmon resonance (SPR) excitation of individual nanoparticles and results in a collective coupled SPR mode of the nanoparticle array. Consequently, a mobile excitation that can hop down the chain to subsequent nanoparticles occurs. Arrays of metal nanoparticles are interesting for the development of optical waveguides, subdiffractional microscopy, bio-chemical sensors, surface-enhanced Raman spectroscopy, and surface-enhanced infrared absorption.

With the rapid development of nanofabrication processing and the progress in the corresponding characterization and measurement technologies, simple nanoparticles such as spherical particles and hybrid nanostructures such as nanoshells[7−13], nanocups, semi-shells, and nanocrescents can be synthesized by physical and chemical methods. Their optical properties have been intensively investigated, and they display promising features such as large tuning ranges for SPRs from near-infrared to ultraviolet wavelengths, high sensitivities against various properties of the surrounding media, and large local field enhancements. Increasing research efforts have also focused on the development of new yet complicated structures such as multi-layer nanoshells[14−19] and composite structures of nanowires and nanoshells[20,21].

Despite several experimental and theoretical attempts to enhance the performance of energy transfer using very different nanoparticle materials, sizes, shapes, and surface coverage, no systematic study has been conducted on optimum light transmission that can be achieved by proper adjustment of nanoparticle parameters, tuning of surface plasmons, and paying attention to the function of higher-order modes in plasmonic enhancements, except for a few reported results[9,22]. Thus, finding the optimum nanoparticle parameter space to enable effective plasmon enhancement, especially by tuning the higher-order surface modes, remains one of the major challenges in this field. In this letter, we present a systematic study on the transmission properties and the near-field plasmonic behaviors of coaxial gold nanotube arrays by using the finite-difference time-domain (FDTD) method[23]. The near-field optical response, intensity, position, and linewidth of the SPR peaks can be tuned over a wide range merely by manipulating the geometry and dielectric parameters.

The model we simulated is depicted in Fig. 1, where linear chains with nine nanotubes are considered. For our simulations, the outer and inner radii of the outer-layer gold nanotubes are denoted by R_1 and R_2. The thickness of the outer tube is denoted by $d_1 = R_2 - R_1$; the outer and inner radii of the inner gold nanotubes are denoted by R_3 and R_4; the thickness of the outer tube is denoted by $d_2 = R_3 - R_4$; the separation between the two layers is denoted by $\Delta = R_2 - R_3$; the intertube spacing between neighbor coaxial nanotube g is set to 20 nm; the refractive medium dielectric parameter from outside to inside isdepicted by ε_1, ε_3, and ε_5, respectively. The calculated region is truncated by using a perfectly matched layer absorbing the boundary conditions on the left and right surfaces of the computational space along the x direction. Periodic boundary conditions are applied along the y direction due to the periodicity of the structure. We then send a Gaussion single pulse of light with a wide frequency profile. The incident light is along the x direction with TM polarization.

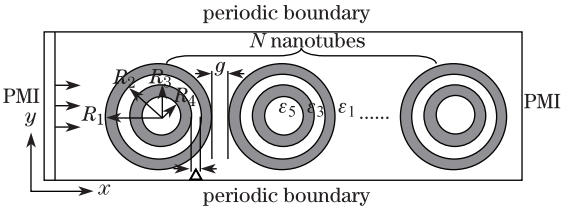

Fig. 1. Top view of the infinitely long coaxial gold nanotube arrays with nine nanotubes.

The frequency-dependent optical properties of the gold nanostructure are approximated by the Drude model, which defines dispersive permittivity as $\varepsilon(\omega) = 1 - \frac{\omega_p^2}{\omega^2 + i\omega\gamma}$, where $\omega_p = 1.37 \times 10^{16}$ s^{-1} is the bulk plasmon frequency of the gold, ω is the angle frequency of the incident wave, and γ=4.08×10^{13} s^{-1} represents the damping rate that characterizes the ohmic absorption loss. The values are obtained by fitting the experimental results[24]. We simulated the structure with a FDTD cube with size $L_x \times L_y$ =1 240 × 140 (nm) infinitely along the z direction. The two dimensional (2D) structure shows similar physical phenomena to those of the three dimensional (3D) structure, so 2D nanostructures are used to investigate the dependence of electric and mechanical properties on dimensionality and size reduction; they can also be used as nano-interconnects and nano-functional units in optoelectronic, electronic, electrochemical, and electromechanical devices. We mainly discuss the 2D structures in this letter. The spatial and temporal steps are set as $\Delta x = \Delta y$=1 nm and $\Delta t = \Delta x/2c$ (where c is the velocity of light in vacuum).

The thickness of the nanotube has an important function in determining the plasmon resonance properties of the metallic nanotube array[11]. We first consider the thickness influence of the outer tube, as observed from Fig. 2, varying the d_1 from 5, 10 or 15 nm for fixed d_2=10 nm and Δ = 20 nm. We keep R_1=50 nm constant all throughout, so when the outer tube thickens, R_2, R_3, and R_4 all decrease. Two distinct transmission bands are clearly observed. The bands at shorter wavelengths are a combination of resonances due to higher-order multipole modes. Two forbidden band gaps are also present. With the increase in the thickness of the outer tube, the transmission spectra noticeably blue shift. The split transmission band in the visible region merges and narrows down, that in the near-infrared region is enhanced, and more resonance peaks exist. These findings are similar to those observed in the single-wall nanotube array. Meanwhile, the two forbidden band gaps narrow down, indicating that the working peak wavelengths can be manipulated from visible light to near-infrared by decreasing d_1.

We next study the influence of the thickness of the inner tube. From Fig. 3, along with the increase of inner tube thickness d_2 from 5, 10, or 15 nm, for fixed d_1=10 nm and Δ = 20 nm, the resonance peaks of the transmission peaks in the near-infrared region slightly blue shift and are widened and enhanced. The transmission bands in the visible region noticeably blue shift, are widened and enhanced, and additional irregular splits exist on the left. The band gap in the visible region widens, whereas the band gap in the ultraviolet region narrows down. These results can be ascribed to the thinning of the metal layers and the stronger interaction of plasmons, leading to stronger and narrower resonances. By contrast, the structures with thicker metal layers possess broader peaks[16].

The thickness of the dielectric space layer Δ controls the strength of the coupling between the inner and the outer gold nanotubes. The resulting plasmon energy shifts depend on the coupling strength and the energy between the plasmon on the inner and outer shells. Figure 4 demonstrates that the peak position and the peak intensities are very sensitive to the separation. When Δ= 5 nm, two forbidden band gaps are observed, a very wide transmission band with six resonance peaks expand to the visible and near-infrared region, and a very narrow transmission band exists in the near-infrared region. All the transmission spectra noticeably blue shift, the shorter wavelength resonance peaks and the band gap rapidly narrow down, the peak intensities attenuate, and the number of peaks decreases as the dielectric layer thickness increases from Δ = 5 to 15 nm. The longer wavelength transmission band and band gap exhibit the opposite behavior. When Δ is further increased from 20, 25, or 30 nm, the transmission band in the near-infrared region continues to slightly blue shift, whereas the transmission band in the visible region splits and becomes more irregular. The band gap in the ultraviolet region disappears when Δ=30 nm. The other forbidden band gap almost expands to the whole visible region. Despite the evident advantage of using small separation nanotube arrays for enhanced transmission of the visible light, larger separation offers another distinctive advantage: the peak in the infrared region is wider than those of the smaller separation cases. The results can be ascribed to the thicker dielectric layer that lowers the strength of interplasmon resonance coupling between the inner and outer shells.

From the discussion, we find that the shorter wavelength transmission band is very sensitive to the modification of these parameters, especially when the separation is changed; this result is similar to that of

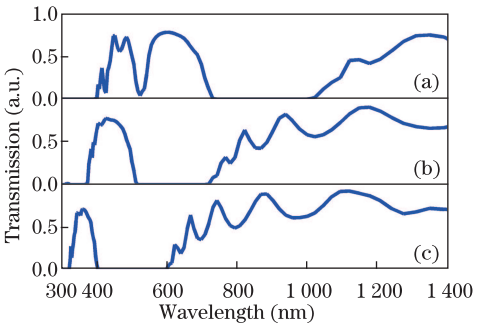

Fig. 2. Transmission spectra through the coaxial nanotubes array as a function of wavelength for R_1= 50 nm, Δ=20 nm, and g=20 nm, with different outer tube thicknesses (a) d_1=5, (b) d_1=10, and (c) d_1=15 nm.

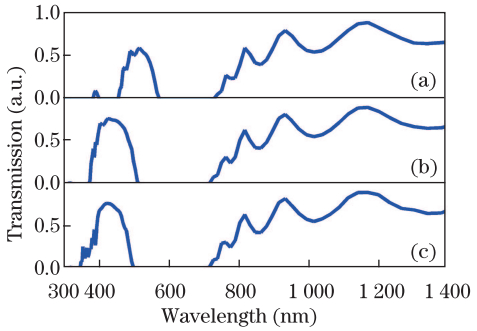

Fig. 3. Transmission spectra through the coaxial nanotubes array as a function of wavelength for R_1=50 nm, R_2=40 nm, R_3=20 nm, Δ=20 nm, and g=20 nm, with different inner tube thicknesses (a) d_2=5, (b) d_2=10, and (c) d_2=15 nm.

the single coaxial nanotubes[17].

To understand the phenomenon of plasmon resonances, we draw the spatial distributions of the E_x field for the resonance modes closest to the left of the shorter and longer wavelength band gaps in Fig. 4(c), as shown in Figs. 5(a)–(d). When d_1=5 nm, the E_x field distribution at λ =415 nm is shown in Fig. 5(a). The octupole modes exist outside the outer tubes and the quadrupole modes appear between the inner and outer tubes and inside the inner tubes. Every three adjacent coaxial nanotubes couple together, which explains the enhanced shorter wavelength transmission band shown in Fig. 2(a). The E_x field distribution at λ =327 nm (d_1=15 nm) is depicted in Fig. 5(b). The hexapole plasmon modes exist outside the outer tubes. A dipole or quadrupole mode emerges between the inner and outer tubes and inside the inner tube. The coupling strength between adjacent coaxial tubes is very weak compared with that in a thinner case, which explains the attenuation of the transmission band as thickness increases. Unlike the case for shorter wavelength, no obvious electric field exists inside the inner tube. Quadrupole modes exist between and outside the outer tubes as shown in Fig. 5(c) at λ =1 346 nm (d_1=5 nm). The field predominantly distributes in between the gap regions of the coaxial nanotube, and the local fields of adjacent nanotubes are coupled together and produce highly enhanced evanescent fields as shown in Fig. 5(d) at λ=622 nm (d_1=15 nm). These findings indicate that the lower energy modes mostly result from the hybridization plasmon of the adjacent coaxial nanotubes. The near-field intensities of local fields in the gaps between adjacent coaxial nanotubes are quite sensitive to the thickness of the outer tubes. When varying d_1 from 5 to 15 nm, the high-energy mode weakens and the low-energy mode becomes strong, which explains the narrowing of the transmission band in the visible region and the widening of the transmission band in the near-infrared region.

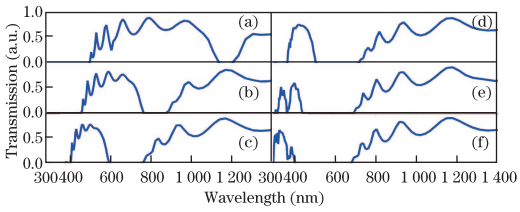

Fig. 4. Transmission spectra through the coaxial nanotube array as a function of wavelength for d_1=d_2=10 nm and g=20 nm, with different separations between two tubes, where Δ are (a) 5, (b) 10, (c) 15, (d) 20, (e) 25, and (f) 30 nm, respectively.

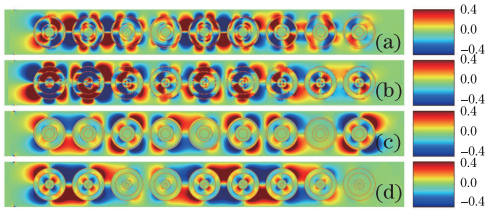

Fig. 5. Instantaneous electric field distribution at different resonance peak wavelengths as presented in Fig. 2: (a) λ=415 nm (d_1=5 nm), (b) λ=327 nm (d_1=15 nm), (c) λ=1346 nm (d_1=5 nm), and (d) λ=622 nm (d_1=15 nm).

The plasmon resonance frequency of the nanoshell is extremely sensitive to surrounding dielectric media, holding great potential for monitoring localized environmental changes during chemical and biological processes. We investigate the dielectric environment effects on the optical transmission properties.

Firstly, Figs. 6(a)–(c) depict the transmission spectra of the coaxial nanotube array with various surrounding environment dielectric parameters ε_1= 1, 2, and 3, with fixed ε_3=ε_5 =1, d_1 = d_2=10 nm, Δ=20 nm, and g=20 nm. Compared with Fig. 6(a) (ε_1=ε_3=ε_5 = 1), with the increase of ε_1, the transmission spectra are largely modified, the peak intensities of the two transmission bands sharply decrease and red shift, and the transmission band in the near-infrared region shifts more, so the band gap between them remarkably widen. The results are analogous to those observed in the square-core metallic nanotube array[12].

We further consider the dielectric parameter influence of the embedding media between the inner and outer layer tubes. As shown in Figs. 7(a)–(f), when ε_3 is increased from 1 to 6 with ε_1=ε_5 =1, d_1 = d_2=10 nm and Δ=20 nm are unchanged and the transmission spectra monotonically red shifts. The band gap in the ultraviolet region expands to the visible region, and the band gaps in the visible region shift to the near-infrared region and narrow down. The transmission bands in the visible region sharply broaden and expand to the near-infrared region, and more peaks appear. When ε_3 is bigger than 4, some dense and irregular peaks exist in the ultraviolet region, and the intensities of the high-energy transmission band are enhanced with further increase in ε_3.

In Figs. 8 (a)–(f), we draw the transmission spectra of the varied core dielectric parameters inside the inner tubes. When ε_5 increases from 1 to 6, the intensity and position of peaks of the transmission band in the near-infrared region remain almost unchanged. The transmission band in the visible region red shifts, sharply weakens, and changes from multi-peak to single-peak spectra. When ε_5 is bigger than 3, some new irregular peaks exist in the band gaps in the ultraviolet region.

The main effect of the dielectric media on the optical properties of the nanotube is ascribed to the polarization of the dielectric. When the nanotube is placed in a time-dependent external field, the dielectrics polarize and produce an additional component to the excitation field across the nanotube. The electrons screen the

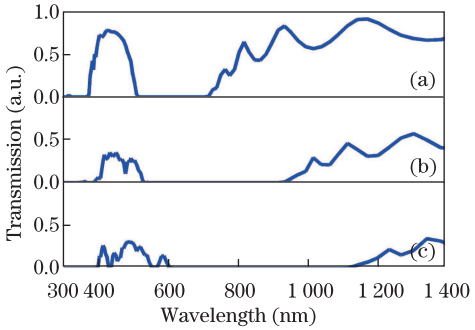

Fig. 6. Transmission spectra through the coaxial nanotube array as a function of wavelength for d_1 = d_2=10 nm, Δ=20 nm, g=20 nm, and ε_3=ε_5=1 with different ε_1, (a) 1, (b) 2, and (c) 3.

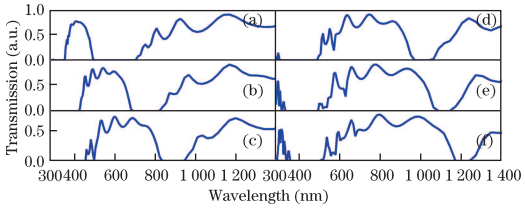

Fig. 7. Transmission spectra through the coaxial nanotube array as a function of wavelength for $d_1 = d_2$=10 nm, Δ=20 nm, g=20 nm, and ε_1=ε_5=1 with different ε_3, (a) 1, (b) 2, (c) 3, (d) 4, (e) 5, and (f) 6.

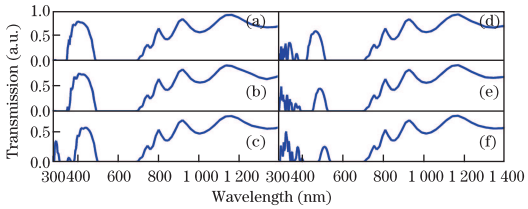

Fig. 8. Transmission spectra through the coaxial nanotube array as a function of wavelength for $d_1 = d_2$=10 nm, Δ=20 nm, g=20 nm, and ε_1=ε_3=1 with different ε_5, (a) 1, (b) 2, (c) 3, (d) 4, (e) 5, and (f) 6.

original excitation field and the field produced by the dielectric[13]. When the nanotube arrays are embedded in a dielectric medium, the dielectric effect is much larger because it polarizes in response to the resulting field, thereby more effectively reducing the strength of the surface charges outside of the nanotubes and leading to a decreased restoring force; consequently, the plasmon energies are lowered[13], which explains the sharp weakening of the transmission spectra as ε_1 increases. The dielectric layer between the metal layers and the dielectric polarization cause the symmetric and anti-symmetric plasmon resonances to shift to lower energies. Thus, the transmission spectra red shift when ε_3 is increased. More electric charges exist outside the outer-tube surface (not shown), so the coupling between adjacent coaxial tubes intensifies, resulting in the enhancement of the transmission band in the visible region. The effect of the dielectric core on the electronic structure of the nanotube is very weak, but when the dielectric parameter is sufficiently high, more electric charges will exist between and in the inner tube (not shown). The plasmon coupling between the adjacent coaxial tube weakens, so the shorter-wavelength transmission band attenuates.

In conclusion, we show that coupled coaxial nanotube arrays exhibit tunable plasmon resonances properties, enhanced transmission, and a wide forbidden band gap. The plasmonic behaviors and spectral responses can be tuned by a rational selection of the outer and inner thicknesses of the nanotubes, the separation between the double-layer nanotube, and the dielectric parameters of the embedding media. Our chain waveguide can be easily tailored for different operation wavelengths, ranging from ultraviolet to near-infrared, because of the large tunability of the coaxial nanotube arrays. Based on the E_x electric field distribution, the antisymmetric quadrupolar plasmon modes exist in the longer-wavelength transmission bands, whereas in the shorter ones, higher-order modes and symmetric quadrupolar plasmon modes are present. The higher-order modes become more important when the separation and the dielectric parameter increase. This simulation result may be used to design structures with optimized nano-photonic devices for waveguides, interferometers or other densely integrated plasmonic circuitry.

This work was supported by the Research Fund for the Doctoral Program of Higher Education of China (No. 20100162110068) and the Scientific Research Fund of Hunan Provincial Education Department (No. 10B022).

References

1. M. L. Brongersma, J. W. Hartman, and H. A. Atwater, Phys. Rev. B **62,** R16356 (2000).
2. Q. Wei, K. Su, S. Durant, and X. Zhang, Nano. Lett. **4,** 1067 (2004).
3. D. S. Citrin, Nano. Lett. **4,** 1561 (2004).
4. L. A. Sweatlock, S. A. Maier, H. A. Atwater, J. J. Penninkhof, and A. Polman, Phys. Rev. B **71,** 235408 (2005).
5. F. Le, D. W. Brandl, Y. A. Urzhumov, H. Wang, J. Kundu, N. J. Halas, J. Aizpurua, and P. Nordlander, ACS Nano. **2,** 707 (2008).
6. S. A. Maier, P. G. Kik, and H. A. Atwater, Appl. Phys. Lett. **81,** 1714 (2002).
7. A. O. Pinchuk and G. C. Schatz, Appl. Phys. B **93,** 31 (2008).
8. B. N. Khlebtsov, V. A. Khanadeyev, J. Ye, D. W. Mackowski, G. Borghs, and N. G. Khlebtsov, Phys. Rev. B **77,** 035440 (2008).
9. X. Cui and D. Erni, J. Opt. Soc. Am. A **25,** 1783 (2008).
10. Y. F. Chau, H. H. Yeh, C. Y. Liu, and D. P. Tsai, Opt. Commun. **283,** 3189 (2010).
11. H. Li, S. Fu, H. Xu, S. Xie, X. Zhou, and J. Wu, Opt. Commun. **283,** 3985 (2010).
12. Z. Liu, H. Li, H. Xu, S. Xie, X. Zhou, and C. Wu, Opt. Commun. **284,** 3331 (2011).
13. E. Prodan, A. Lee, and P. Nordlander, Chem. Phys. Lett. **360,** 325 (2002).
14. C. Radloff and N. J. Halas, Nano. Lett. **4,** 1323 (2004).
15. Y. Hu, R. C. Fleming, and R. A. Drezek, Opt. Express **16,** 19579 (2008).
16. A. K. Kodali, M. V. Schulmerich, R. Palekar, X. Llora, and R. Bhargava, Opt. Express **18,** 23302 (2010).
17. H. Xu, H. Li, Z. Liu, S. Xie, X. Zhou, and J. Wu, Solid State Commun. **151,** 759 (2011).
18. D. Wu and X. Liu, Appl. Phy. Lett. **96,** 151912 (2010).
19. H. Khosravi, N. Daneshfar, and A. Bahari, Phys. Plasmas **17,** 053302 (2010).
20. Y. F. Chau, Y. J. Lin, and D. P. Tsai, Opt. Express **18,** 3510 (2010).
21. Y. F. Chau, Z. H. Jiang, H. Y. Li, G. M. Lin, F. L. Wu, and W. H. Lin, Progress In Electromagnetics Research B **28,** 183 (2011).
22. Y. A. Akimov, W. S. Koh, and K. Ostrikov, Opt. Express **17,** 10195 (2009).
23. A. Taflove and S. C. Hagness, *Computational Electrodynamics*: *The Finite-Difference Time-Domain Method,* 2nd edn. (Artech House, Boston, 2000).
24. E. D. Palik, *Handbook of Optical Constants in Solids* (Academic, Boston, 1982).